Visual Understanding of Light Absorption and Waveguiding in Standing Nanowires with 3D Fluorescence Confocal Microscopy

Rune Frederiksen,[†] Gozde Tutuncuoglu,[‡] Federico Matteini,[‡] Karen L. Martinez,[†] Anna Fontcuberta i Morral,[‡] and Esther Alarcon-Llado*,[‡,§]

[†]Bio-Nanotechnology and Nanomedicine Laboratory, Department of Chemistry & Nano-Science Center, University of Copenhagen, Universitetsparken 5, DK-2100 Copenhagen, Denmark
[‡]Laboratory of Semiconductor Materials, Institute of Materials, School of Engineering, EPFL, 1015 Lausanne, Switzerland
[§]Center for Nanophotonics, AMOLF, Science Park 104, 1098XG Amsterdam, The Netherlands

S *Supporting Information*

ABSTRACT: Semiconductor nanowires are promising building blocks for next-generation photonics. Indirect proofs of large absorption cross sections have been reported in nanostructures with subwavelength diameters, an effect that is even more prominent in vertically standing nanowires. In this work we provide a three-dimensional map of the light around vertical GaAs nanowires standing on a substrate by using fluorescence confocal microscopy, where the strong long-range disruption of the light path along the nanowire is illustrated. We find that the actual long-distance perturbation is much larger in size than calculated extinction cross sections. While the size of the perturbation remains similar, the intensity of the interaction changes dramatically over the visible spectrum. Numerical simulations allow us to distinguish the effects of scattering and absorption in the nanowire leading to these phenomena. This work provides a visual understanding of light absorption in semiconductor nanowire structures, which is of high interest for solar energy conversion applications.

KEYWORDS: semiconductor nanowire, optical properties, solar energy, confocal microscopy
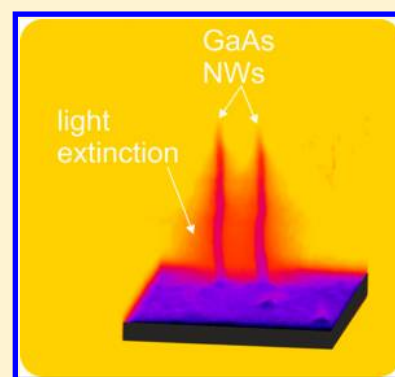
Since the discovery of photonic properties of dielectric nanostructures,[1−7] their great potential for solar applications at lower cost has been unraveled.[8−18] Nanowire (NW) ensembles constitute a new class of metamaterial, where the optical properties cannot be directly deduced from individual parts.[19−22] Optical properties of NW arrays are tuned by the individual NW type, geometry, and collective arrangement, which provide a new playground in solar energy conversion and the solid-state lighting arenas.[23−32] The effective absorption cross section in vertically standing nanowires can be much larger than the geometrical one.[6,8,33] This large absorption cannot be explained by the standard Mie-like resonance formulism, as in the case of horizontally lying structures.[34,35] Assessing the absorption cross section in vertical structures is not straightforward, and it is important to understand how light is interacting with nanostructures and essential for the accurate quantum efficiency determination in photodevices. Many approaches have been shown to measure the optical local density of states in and around photonic and plasmonic structures, which include cathodoluminescence tomography,[36] near-field optical probe techniques, single molecules attached to an AFM tip,[37,38] or fluorescent solutions probed with super-resolution microscopes,[39−41] among others. Although complex computational work has shown that super-resolution micros-copy can be used to scan in all three dimensions,[42] no studies

have shown 3D imaging of local density of states at microscale surroundings of photonic nanostructures.

In this work, we are interested in the 3D visualization of long-range light−matter interactions in gallium arsenide (GaAs) standing nanowires, in particular within the region of large absorption. To this end, we use a simple confocal microscope setup. The reconstructed fluorescence image captures the evolution of light extinction around the nanowire and along its length. By combining the experiments with electromagnetic simulations, we elucidate the mechanisms behind self-concentrating light effects and large absorption cross sections found in semiconductor nanowires and their relation to the nanowire waveguiding properties. While the resolution is diffraction limited, we show that this method provides insightful 3D extinction maps around nanostructures, which can be an asset to characterize more complex morphologies.

To demonstrate the power of the technique, we probe GaAs nanowires vertically standing on a silicon (Si) substrate. GaAs is a compound semiconductor with a direct band gap of 1.42 eV, which makes it an excellent candidate for solar energy applications.

Figure 1a illustrates the experimental setup that provides a three-dimensional mapping of light distribution around
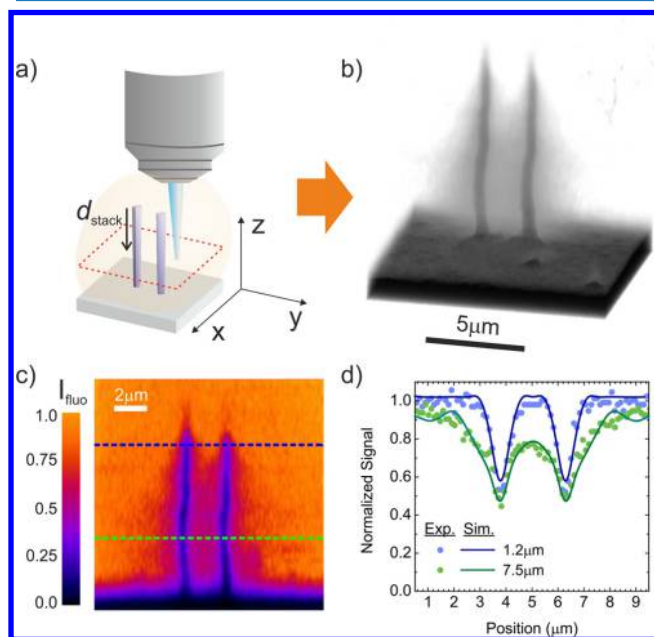
Figure 1. (a) Schematic illustration of the measurement setup and (b) a 3D reconstruction of the optical density in an area around two GaAs NWs on silicon illuminated with blue light (λ = 488 nm) obtained by confocal microscopy. The nanowires are 10 μm long with a diameter of 126 nm and 2.5 μm apart. (c) Orthogonal cross-section fluorescence intensity plot of the same image as in (b). Fluorescence intensity is normalized to that observed far from the nanowires. Dotted lines indicate the set of data points represented in (d). (d) Line-scan profiles experimentally obtained at 1.2 and 7.5 μm below the nanowire tip (dots). Thick lines correspond to the simulated light intensity, by considering light with random polarization and convoluting the data with a Gaussian point spread function.

nanostructures. The sample is embedded in a liquid solution with suspended fluorescent dye molecules (see Supporting Information S1 for more details). The dye fluorescence intensities are mapped around the nanowires with a laser scanning confocal microscope. Dye molecules are excited with a laser beam focused with a confocal microscope objective, and the emitted light is collected through the same objective and detected with a photomultiplier (PMT). The physical principle of this characterization method resides in the fluorescence intensity of the molecules being proportional to the local excitation light intensity. Thus, by scanning the laser beam over an x–y area for a number of z-stacks, a diffraction-limited resolution 3D map of the light intensity is obtained. The x–y and z optical resolution in our experiments is specified in the Supporting Information.

An example of a reconstructed 3D image of light around GaAs nanowires when illuminated with blue laser light is shown in Figure 1b. In this case, two vertical GaAs nanowires (10 μm long, 126 nm in diameter, and 2.5 μm apart) stand vertically on a Si substrate. The sample is excited with blue light (λ = 488 nm), for which theory predicts that it should not have the strongest interaction with these nanostructures (see Supporting Information on the absorption spectrum of a single nanowire). The represented gray transparency in the image is linked to the amount of detected light, so that the darkest areas in the image indicate positions where no light is detected. As a consequence, the substrate appears dark. Under these conditions, also two dark columns stand at the position of the nanowires and a dark layer where the silicon substrate starts, in accordance with the lack of fluorophores in that volume. Interestingly, a semi-transparent conical region surrounds the nanowires and widens up to several micrometers when approaching the nanowires' bottom. The y–z cross-section intensity contour plot of the same image (Figure 1c) provides a more quantitative representation of the conical "shadow". These pictures represent a clear visual image of how the nanowire pair is
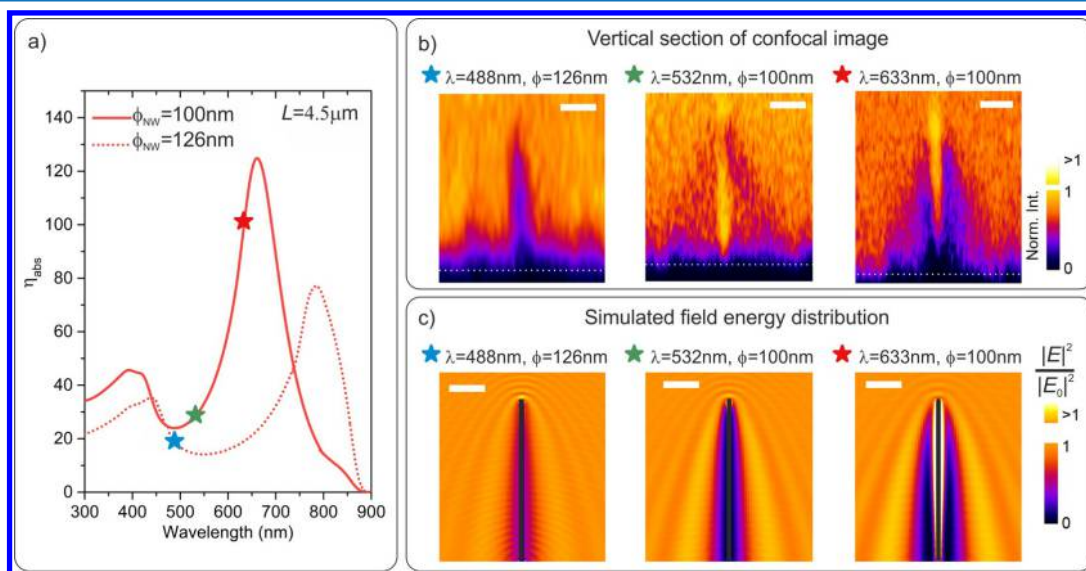
Figure 2. (a) Calculated absorption efficiency spectrum for a 4.5-μm-long vertical GaAs nanowire in water. Two nanowire diameters (ϕ_{NW}) are shown. Stars correspond to the experimental conditions used. (b) Orthogonal cross-sectional confocal images of GaAs nanowires obtained with 488, 532, and 633 nm excitation wavelengths (from left to right, respectively). The intensity is normalized to that far from the nanowires. Dotted line indicates the substrate surface (c) FDTD-simulated field energy distribution for the three geometries described above (ϕ_{NW} = 100 or 126 nm and L = 4.5 μm). Here, only the excitation beam is being considered and has been averaged over all polarizations. The nanowire area is shaded as a black rectangle since fluorescent molecules cannot be found inside. Scale bar is 1000 nm.

capable of redistributing the electromagnetic field around them at a long-range distance. It is clear from this picture that there is less light arriving at the silicon substrate surface due to the presence of the nanowires. It is interesting to note both the dimension and the magnitude of the shaded silicon surface. A better understanding of how light is redistributed around the nanowires is discussed later on. First, to confirm and prove that our experimental setup is truly representing the light intensity distribution around the nanowires of the incoming laser, finite-difference time-domain (FDTD) simulations were performed. The steady-state field energy distribution was simulated by considering an incoming plane wave propagating in the $-z$ direction and the same wavelength as in the experiment ($\lambda =$ 488 nm). Due to the asymmetry of the nanowire pair, two sets of simulations were performed for light polarized in the x and y axes, respectively. The resulting intensity maps were averaged to obtain the final distribution map. Figure 1d displays the line profiles of the calculated electric field intensity squared superimposed to the fluorescence light intensity at 1.2 and 7.5 μm below the nanowire tip. The calculated field energy distributions are in remarkable agreement with the detected light distribution from the confocal images. This result confirms that the observed confocal images are indeed an excellent representation of the interaction between a vertically impinging plane wave and the nanostructures, which can span up to several micrometers in distance. Such good agreement also rules out that the confocal image is strongly perturbed by the possible interactions between fluorophore emission and the nanostructures. In fact, light emitted by the fluorophores is perturbed only when very close to the nanowire surface (<12 nm) and is mostly smeared out when convoluting for the point spread function of the microscope.[43,44] See Supporting Information section S3 for more details. Figure 1 illustrates the potential of fluorescence confocal microscopy as an excellent tool to visualize and assess the 3D extinction cross section of high-aspect-ratio nanostructures. Indeed, the resulting confocal images are a combination of all possible interactions of light with the nanostructures, i.e., scattering, waveguiding, and absorption, and their interplay with and relevance to the case of GaAs nanowires is discussed below.

Earlier works have shown that vertical semiconductor nanowires, such as silicon, InP, or GaAs, exhibit absorption efficiencies that are far above 1 and have a strong spectral dependence with absorption peaks unexplained by the bulk optical parameters.[6,8,9,33,45] Here, the absorption efficiency calculated by FDTD as a function of wavelength for two single GaAs nanowires with diameters ϕ_{NW} of 100 and 126 nm is shown in Figure 2a. One can clearly observe two main peaks, the position of which varies with ϕ_{NW}. For the specific diameter of 100 nm, the absorption peak occurs at a wavelength very close to the band gap of GaAs. Even though the extinction coefficient is small in this spectral region, the strong interaction with light from a large area surrounding the NW allows for such extreme absorption. This diameter is particularly important for the design of solar cells. Here we show that the spectral dependence of absorption is basically dictated by the coupling of light into different photonic modes in the nanowire (see refs 33, 34, 46, 47 and the Supporting Information for more details on the contribution of the HE$_{11}$ mode to the total absorption in vertical nanowires). In particular, the main absorption peak at long wavelengths is due to the coupling of light into the HE$_{11}$ guided mode. Such distinct light–matter interactions give rise to large differences in light absorption within small spectral

windows, rendering the vertical nanowire systems particularly challenging to picture how light is being absorbed. This motivates our study of GaAs nanowires at different absorption regimes. Within our experimental constraints, we have used two different sets of nanowire diameters and three different wavelengths, marked by stars in Figure 2a, to span over different absorption efficiency regimes.

Figure 2b shows confocal cross-sectional images of individual GaAs NWs obtained for the conditions just mentioned, for which the absorption efficiency changes by up to a factor of 4. Nanowires of similar lengths ($\sim$4–5 μm) have been chosen. The color scale represents the intensity of detected light normalized to that found far from the nanowire (i.e., the bulk solution). The respective confocal images in Figure 2b exhibit a strong and clear progression when shifting from the small to large absorption conditions. In all cases, we observe the conical shadow as described in Figure 1, but it becomes much darker when approaching the conditions of large absorption. The fact that for certain conditions there is light missing in the nanowire nearby could be an indication that the absorption efficiency in vertically standing nanowires is larger than its physical diameter. In the rightmost image of Figure 2b, the shadow is so intense that light emitted within the shadow and in particular at the nanowire bottom is below our detection limit. It is interesting to note that while the darkness of the shadow has a strong dependence on the absorption regime condition, its extent does not. This is quite striking and indicates that the interaction volume between nanowire and light is not noticeably linked to the absorption cross section; that is, the absorption cross section cannot be directly measured from the extent of the shadow. On the other hand, there is a less intuitive effect observed in the confocal images: the nanowire appears brighter when approaching the absorption peak. In order to understand both effects (darker shadow and brighter nanowire for the high-absorption regime), we show FDTD-simulated field energy distributions for the three nanowire and illumination conditions in Figure 2c. The images have been obtained by simulating a single GaAs nanowire in water with an unpolarized light source. The simulations are not convoluted with the point spread function (PSF) of the microscope, so that we can focus on the physics of the light–nanowire interaction. The simulated maps show the same trend as in the confocal images when approaching the absorption peak: (a) there is a conical region that extends up to several micrometers where the field energy is reduced although its extent is qualitatively the same regardless of illumination conditions; (b) the surface of the nanowire (distances <20 nm) has a strong field concentration. Next we focus on the origin of these two effects and how to relate them with the absorption cross section.

■ RELATION BETWEEN THE DARK CONICAL SHADOW AND ABSORPTION CROSS SECTION

The theory and experimental images from Figure 2 clearly indicate that in the spectral range close to an absorption peak the surroundings of the nanowire become darker with a very characteristic conical geometry. The key question is if this shadow is related to the absorption cross section of a nanowire, and if yes, how?

To answer this question, we focus on how light interacts with a nanowire of a particular diameter and length at the absorption maxima and minima. While absolute values at which wavelengths these maxima/minima occur, the physics is regardless of the nanowire dimensions. Figure 3a shows the calculated
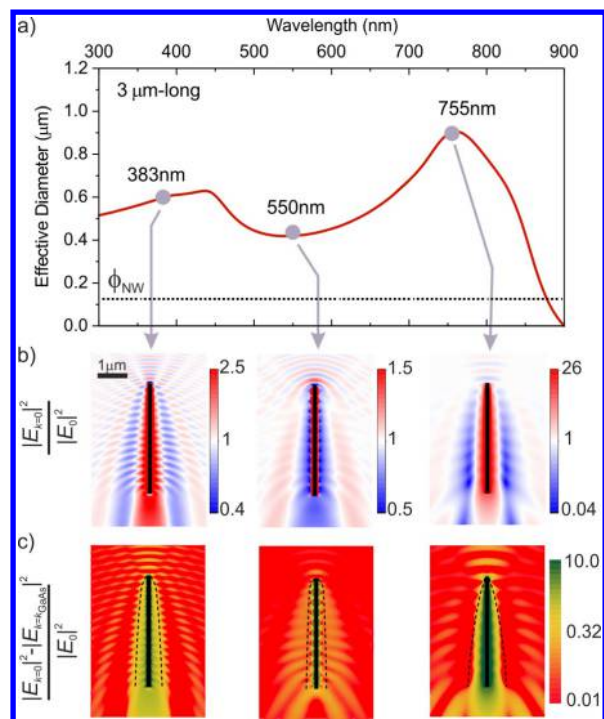
Figure 3. (a) Simulated absorption cross-section diameter as a function of wavelength for a single GaAs nanowire ($L = 3 \mu m$ and ϕ_{NW} = 126 nm). The dashed line corresponds to the physical nanowire diameter. (b) Cross-section representation of the scattered field by assuming no absorption in the GaAs ($L = 3 \mu m$ and ϕ_{NW} = 126 nm). The color bars are in logarithmic scale. The limits have been set to maximize contrast and in such a way that white color is always at a value of 1. (c) Absorption map representation by using the method described in the text. The effective absorption cross-section diameter as a function of length for that particular wavelength is also plotted as dashed curves. The nanowire is represented by the black square, and the scale is kept the same in all maps. All simulations have been polarization averaged.

effective cross-section diameter of a GaAs nanowire with ϕ_{NW} = 126 nm and $L = 3 \mu m$ as a function of wavelength. It is worth noting that the effective diameter of the nanowire is larger than the geometrical one for most of the spectrum, and it is even almost an order of magnitude larger at the absorption peak. To decouple absorption from other contributions, we have simulated the field energy distribution at three characteristic spectral positions for a lossless GaAs nanowire (i.e., the GaAs extinction coefficient, k, is set to 0), $|E_{k=0}|$. The three spectral positions correspond to the main absorption peak at 755 nm, a secondary absorption peak at 383 nm, and the absorption minimum (although still with a cross-section diameter almost 5 times larger than ϕ_{NW}). The color scale in the three $|E_{k=0}|^2$ maps has been set logarithmically, and the scale limits maximize the contrast. When absorption is not taken into account, at 383 and 755 nm (the absorption maxima for the regular GaAs nanowire), a strong field concentration occurs at the surroundings of the nanowire (shown in red), while a shadow (shown in blue) appears at 550 nm (the absorption minimum).

To highlight to what extent absorption is relevant to the confocal images and how much energy is being is dissipated in absorption, we have subtracted the $|E_{k=0}|^2$ map from the field distribution as obtained for a regular GaAs (i.e., by taking absorption into account), $|E_{k=kGaAs}|$. We have normalized the subtraction to the incoming field $((|E_{k=0}|^2 - |E_{k=kGaAs}|^2)/|E_0|^2)$,

and we call the result an absorption map (Figure 3c). The absorption maps at 383 and 755 nm show that most of the light that was scattered and focused at the nanowire is absorbed. We believe that this is related to the coupling to guided modes, whose field is capable of leaking to the far field. For such small nanowire diameters and vertical configuration, most of the visible spectrum will interact with the nanowire via the coupling to its fundamental guided mode.[33,34,46,47] Thus, the absorption spectral dependence is given by the real part of the refractive index (n) instead of the imaginary one (k). Both the refractive index and the diameter of the nanowire define the coupling of light into guided modes. It turns out that the most effective coupling of a plane wave with the nanowire (and consequently the highest absorption) occurs when the guided mode extends outside the boundaries of the nanowire and thus is similar to a weakly guided mode (see Supporting Information). This occurs regardless of the absorption power of the nanowire material. Because of the mode being weakly guided at the absorption maxima, light is poorly confined to the surroundings of the nanowire and creates the light concentration effect seen in Figure 3b. Conversely, if the nanowire can capture those photons, little light can escape, leaving a shadow at the nanowire surroundings.

As a final remark, we notice that in all three conditions represented in Figure 3 the effects of absorption extend several micrometers from the nanowire surface. We compare this to the calculated effective absorption cross section plotted with a dashed line on the absorption maps. The cross section increases with nanowire length, and it saturates to the value given for an infinite GaAs cylinder at lengths longer than ~10 μm (see Supporting Information on absorption dependence on nanowire length). Interestingly, there is not a clear match between the absorption maps and the absorption cross section. In particular a very interesting outcome is that at the absorption minimum, λ = 550 nm, the absorption extends to much larger distances as compared to the cross section. It is worth noting that $(|E_{k=0}|^2 - |E_{k=kGaAs}|^2)/|E_0|^2$ is only about 20% at the nanowire surroundings. In other words, the absorption map shows an extended absorption volume because it is not very effective. By contrast, at the absorption maxima (λ = 383 and 755 nm), the absorption is so effective that it actually extends in the absorption map to a region much smaller than that expected from the cross section.

■ RELATION BETWEEN THE HE$_{11}$ GUIDED MODE AND THE LIGHT INTENSITY AT THE NANOWIRE POSITION

The confocal images show a clear trend of displaying a brighter signal at the nanowire position when increasing the wavelength. We explain this phenomenon with the optical antenna effect; that is, the nanowire collects light from its surroundings and focuses it at the surface.[48] As described in the previous section, the main mechanism by which light interacts with the nanowire is via coupling into guided modes. At short wavelengths ($\lambda/n < \phi_{NW}$) the lowest order mode, HE$_{11}$, is strongly confined to the core of the NW, as shown by the cross-sectional field distribution in Figure 4. In contrast, at longer wavelengths ($\lambda/n > \phi_{NW}$) the mode expands and most of the field intensity resides at the nanowire surface.

Intuitively one would expect that a strong mode confinement to the GaAs leads to strong absorption, desirable for instance in solar cell applications. Still, one should also consider how the incident light can couple into the nanowire. Efficient coupling is
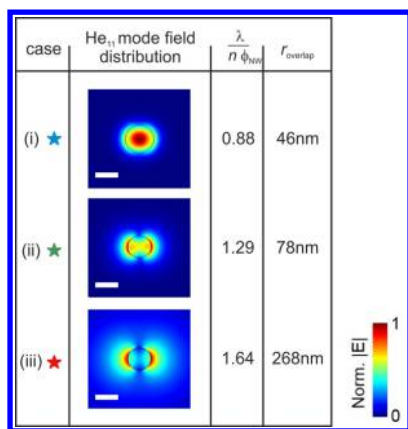
Figure 4. Field distribution given for the HE11 eigenmode in a GaAs infinite cylinder and for the three geometries described in Figure 2. The field has been normalized to its maximum in each plot. The factor Φ_{NW} and radius overlap estimate are listed for all conditions. The scale bar corresponds to 100 nm. The physical boundaries of the nanowire are defined by a black line.

possible when there is a large overlap between the incident field and the field of the photonic modes. When the light source is an extended plane wave, large absorption occurs at wavelengths where the mode is expanded enough to allow efficient incoming light coupling while maintaining enough field energy inside the nanostructure. We assess the area of interaction by defining a radius of overlap, $r_{overlap}$, which is an estimated value of the range of interaction between the photonic mode and the plane wave. The full description of how to calculate $r_{overlap}$ is given in the Supporting Information. The calculated $r_{overlap}$ for the three cases considered here are listed in Figure 4. From case (i) to (iii) $r_{overlap}$ increases dramatically, from 46 nm to 268 nm. In the latter, $r_{overlap}$ is more than 5 times larger than the geometrical radius ($\phi_{NW}/2$) of the nanowire. This is a rough estimate of how much light around the NW is being redistributed into the form of the photonic mode. With this we have highlighted the physical mechanism explaining how light can be collected from an area that is much larger than its physical cross section. This outstanding and nonintuitive property of standing nanowires is also referred to as a self-concentrating effect, which is of major interest for photovoltaic applications and optoelectronics in general. Interestingly, when more light is collected, i.e., case (iii), the strongest field resides at the surface of the NW. As a consequence, fluorophores close to the nanowire surface will be very efficiently excited. Despite the lack of light emission inside the NW volume and the large PSF of the microscope, the strong signal from the surface results in a bright nanowire image. A closer look into this region may be provided by super-resolution microscopes, where the optical resolution is down to a few tenths of a nanometer. However, within this region of strong interaction between the fluorophore and the nanowire, other optical effects start playing a role and the relationship between the detected light and optical density of states is nontrivial.[43,44,49]

It is also worth mentioning that under strong coupling conditions emitted light from fluorophores close to the surface does also efficiently couple to the nanowire via the near field. In those cases, one must also take into account the effects of the nanowire presence on the emitted fluorescent light for a thorough quantitative assessment of the electromagnetic field distribution or density of states close to the nanowire surface.

Effects on the emission quantum yield and in/out-coupling of the emission into/out of the nanowire must be considered, as shown in detail in refs 44, 50, and 51.

In conclusion, we present a method that provides visual information in 3D on the light distribution around nanostructures. In particular, we show that it allows understanding how light travels and is being absorbed in vertical semiconductor nanostructures. For the case of GaAs vertical nanowires, we observe a conically shaped large extinction volume around the nanostructure for wavelengths close to the absorption maximum. We find that the light–nanowire interaction is mainly due to coupling of light into weakly guided modes. The weaker it is, the strongest the absorption and the darker the shadow around the nanowires. This is true up to an optimal absorption wavelength. For longer wavelengths the field is no longer inside the nanowire and thus cannot absorb light. Despite the strong dependence of absorption and radius overlap on wavelength, we observe that light is perturbed in the micrometer range around GaAs nanowires, regardless of the strength of the nanowire absorbing power. This result is very relevant when designing nanowire-based tandem solar cells, as it affects the direction and amount of light arriving at the subsequent cells. This method opens the path toward the investigation of the optical properties of more complex nanostructures and/or metamaterials.

■ ASSOCIATED CONTENT

Ⓢ Supporting Information

The Supporting Information is available free of charge on the ACS Publications website at DOI: 10.1021/acsphotonics.7b00434.

> Experimental details, FDTD simulations setup, derivation of the single nanowire absorption via coupling to the HE11 mode and its length dependence, definition of $r_{overlap}$ and effective absorption cross section (PDF)

■ AUTHOR INFORMATION

Corresponding Author

*E-mail: e.alarconllado@amolf.nl.

ORCID Ⓘ

Anna Fontcuberta i Morral: 0000-0002-5070-2196

Esther Alarcon-Llado: 0000-0001-7317-9863

Notes

The authors declare no competing financial interest.

■ ACKNOWLEDGMENTS

■ REFERENCES

(1) Wang, J.; Gudiksen, M.; Duan, X.; Cui, Y.; Lieber, C. Highly Polarized Photoluminescence and Photodetection from Single Indium Phosphide Nanowires. *Science (Washington, DC, U. S.)* **2001**, *293*, 1455.

(2) Nobis, T.; Kaidashev, E. M.; Rahm, A.; Lorenz, M.; Grundmann, M. Whispering Gallery Modes in Nanosized Dielectric Resonators with Hexagonal Cross Section. *Phys. Rev. Lett.* **2004**, *93*, 103903.

(3) Cao, L.; Nabet, B.; Spanier, J. E. Enhanced Raman Scattering from Individual Semiconductor Nanocones and Nanowires. *Phys. Rev. Lett.* **2006**, *96*, 157402.

(4) Cao, L.; White, J. S.; Park, J.-S.; Schuller, J. a; Clemens, B. M.; Brongersma, M. L. Engineering Light Absorption in Semiconductor Nanowire Devices. *Nat. Mater.* **2009**, *8*, 643−647.

(5) Khudiyev, T.; Ozgur, E.; Yaman, M.; Bayindir, M. Structural Coloring in Large Scale Core-Shell Nanowires. *Nano Lett.* **2011**, *11*, 4661−4665.

(6) Wu, P. M.; Anttu, N.; Xu, H. Q.; Samuelson, L.; Pistol, M. Colorful InAs Nanowire Arrays: From Strong to Weak Absorption. *Nano Lett.* **2012**, *12*, 1990.

(7) Van Dam, D.; Abujetas, D. R.; Sánchez-gil, J. A.; Haverkort, J. E. M.; Bakkers, E. P. A. M.; Gomez-Rivas, J. Strong Diameter-Dependence of Nanowire Emission Coupled to Waveguide Modes Strong Diameter-Dependence of Nanowire Emission Coupled to Waveguide Modes. *Appl. Phys. Lett.* **2016**, *108*, 121109.

(8) Krogstrup, P.; Jørgensen, H. I.; Heiss, M.; Demichel, O.; Holm, J. V.; Aagesen, M.; Nygard, J.; Fontcuberta I Morral, A. Single-Nanowire Solar Cells beyond the Shockley−Queisser Limit. *Nat. Photonics* **2013**, *7*, 306−310.

(9) Wallentin, J.; Anttu, N.; Asoli, D.; Huffman, M.; Aberg, I.; Magnusson, M. H.; Siefer, G.; Fuss-Kailuweit, P.; Dimroth, F.; Witzigmann, B.; et al. InP Nanowire Array Solar Cells Achieving 13.8% Efficiency by Exceeding the Ray Optics Limit. *Science* **2013**, *339*, 1057−1060.

(10) Yao, M.; Huang, N.; Cong, S.; Chi, C.-Y.; Seyedi, M. A.; Lin, Y.-T.; Cao, Y.; Povinelli, M. L.; Dapkus, P. D.; Zhou, C. GaAs Nanowire Array Solar Cells with Axial P-I-N Junctions. *Nano Lett.* **2014**, *14*, 3293.

(11) Mariani, G.; Scofield, A. C.; Hung, C.-H.; Huffaker, D. L. GaAs Nanopillar-Array Solar Cells Employing in Situ Surface Passivation. *Nat. Commun.* **2013**, *4*, 1497.

(12) Mann, S.; Oener, S.; Cavalli, A.; Haverkort, J. E. M.; Bakkers, E. P. A. M.; Garnett, E. Quantifying Losses and Thermodynamic Limits in Nanophotonic Solar Cells. *Nat. Nanotechnol.* **2016**, DOI: 10.1038/nnano.2016.162.

(13) Piper, J. R.; Fan, S. Broadband Absorption Enhancement in Solar Cells with an Atomically Thin Active Layer. *ACS Photonics* **2016**, *3*, 571−577.

(14) Huang, N.; Lin, C.; Povinelli, M. L. Broadband Absorption of Semiconductor Nanowire Arrays for Photovoltaic Applications. *J. Opt.* **2012**, *14*, 024004.

(15) Diedenhofen, B. S. L.; Vecchi, G.; Algra, R. E.; Hartsuiker, A.; Muskens, O. L.; Immink, G.; Bakkers, E. P. A. M.; Vos, W. L.; Gomez-Rivas, J. Broad-Band and Omnidirectional Antireflection Coatings Based on Semiconductor Nanorods. *Adv. Mater.* **2009**, *21*, 973−978.

(16) Muskens, O. L.; Rivas, J. G.; Algra, R. E.; Bakkers, E. P. A. M.; Lagendijk, A. Design of Light Scattering in Nanowire Materials for Photovoltaic Applications. *Nano Lett.* **2008**, *2*, 263810.1021/nl0808076.

(17) Zhu, J.; Cui, Y. More Solar Cells for Less. *Nat. Mater.* **2010**, *9*, 183−184.

(18) Vescovi, G.; Asoli, D.; Naseem, U.; Gilboy, J. P.; Sundvall, C.; Dahlgren, A.; Svensson, K. E.; Anttu, N.; Bj, M. T.; Samuelson, L. A GaAs Nanowire Array Solar Cell With 15. 3%. *IEEE J. Photovoltaics* **2016**, *6*, 185.

(19) Seo, K.; Wober, M.; Steinvurzel, P.; Schonbrun, E.; Dan, Y.; Ellenbogen, T.; Crozier, K. B. Multicolored Vertical Silicon Nanowires. *Nano Lett.* **2011**, *11*, 1851−1856.

(20) Lee, W.; Senanayake, P.; Farrell, A. C.; Lin, A.; Hung, C.; Huffaker, D. L. High Quantum Efficiency Nanopillar Photodiodes Overcoming the Diffraction Limit of Light. *Nano Lett.* **2016**, *16*, 199.

(21) Mann, S.; Grote, R.; Osgood, R. M.; Alu, A.; Garnett, E. Opportunities and Limitations for Nanophotonic Structures to Exceed the Shockley-Queisser Limit. *ACS Nano* **2016**, *10*, 862010.1021/acsnano.6b03950.

(22) Heiss, M.; Russo-Averchi, E.; Dalmau Mallorquí, a.; Tütüncüoğlu, G.; Matteini, F.; Rüffer, D.; Conesa-Boj, S.; Demichel, O.; Alarcon-Lladó, E.; Fontcuberta I Morral, A. III-V Nanowire Arrays: Growth and Light Interaction. *Nanotechnology* **2014**, *25*, 01401510.1088/0957-4484/25/1/014015.

(23) Brongersma, M. L.; Cui, Y.; Fan, S. Light Management for Photovoltaics Using High-Index Nanostructures. *Nat. Mater.* **2014**, *13*, 451−460.

(24) Cao, L.; Fan, P.; Vasudev, A. P.; White, J. S.; Yu, Z.; Cai, W.; Schuller, J. a; Fan, S.; Brongersma, M. L. Semiconductor Nanowire Optical Antenna Solar Absorbers. *Nano Lett.* **2010**, *10*, 439−445.

(25) Samuelson, L. III-V and III-Nitride Nanowires for LED Applications. *Lasers Electro-Optics Eur. (CLEO Eur.. 2013 Conf. Int. Quantum Electron. Conf.* **2013**, 110.1109/CLEOE-IQEC.2013.6800944.

(26) Liu, C.; Dasgupta, N.; Yang, P. Semiconductor Nanowires for Artificial Photosynthesis. *Chem. Mater.* **2013**, *26*, 415.

(27) Hu, S.; Chi, C.-Y.; Fountaine, K. T.; Yao, M.; Atwater, H. a.; Dapkus, P. D.; Lewis, N. S.; Zhou, C. Optical, Electrical, and Solar Energy-Conversion Properties of Gallium Arsenide Nanowire-Array Photoanodes. *Energy Environ. Sci.* **2013**, *6*, 1879−1890.

(28) Gao, L.; Cui, Y.; Vervuurt, R. H. J.; Van Dam, D.; Van Veldhoven, R. P. J.; Hofmann, J. P.; Bol, A. A.; Haverkort, J. E. M.; Notten, P. H. L.; Bakkers, E. P. A. M.; et al. High-Efficiency InP-Based Photocathode for Hydrogen Production by Interface Energetics Design and Photon Management. *Adv. Funct. Mater.* **2016**, *26*, 679−686.

(29) Fountaine, K. T.; Kendall, C. G.; Atwater, H. A. Near-Unity Broadband Absorption Designs for Semiconducting Nanowire Arrays via Localized Radial Mode Excitation. *Opt. Express* **2014**, *22*, A930.

(30) Tian, B.; Zheng, X.; Kempa, T. J.; Fang, Y.; Yu, N.; Yu, G.; Huang, J.; Lieber, C. M. Coaxial Silicon Nanowires as Solar Cells and Nanoelectronic Power Sources. *Nature* **2007**, *449*, 885−889.

(31) Guan, N.; Dai, X.; Messanvi, A.; Zhang, H.; Yan, J.; Gautier, E.; Bougerol, C.; Julien, F.; Durand, C.; Eymery, J.; et al. Flexible White Light Emitting Diodes Based on Nitride Nanowires and Nano-phosphors. *ACS Photonics* **2016**, *3*, 597.

(32) Mann, S. A.; Grote, R. R.; Osgood, R. M.; Alu, A.; Garnett, E. Opportunities and Limitations for Nanophotonic Structures To Exceed the Shockley−Queisser Limit. *ACS Nano* **2016**, *10*, 8620.

(33) Mokkapati, S.; Saxena, D.; Tan, H. H.; Jagadish, C. Optical Design of Nanowire Absorbers for Wavelength Selective Photo-detectors. *Sci. Rep.* **2015**, *5*, 15339.

(34) Grzela, G.; Paniagua-Dominguez, R.; Barten, T.; Van Dam, D.; Sanchez-Gil, J.; Gomez-Rivas, J. Nanowire Antenna Absorption Probed with Time-Reversed Fourier Microscopy. *Nano Lett.* **2014**, *14*, 3227.

(35) Abujetas, D. R.; Paniagua-Dominguez, R.; Sanchez-Gil, J. Unraveling the Janus Role of Mie Resonances and Leaky/Guided Modes in Semiconductor Nanowire Absorption for Enhanced Light Harvesting. *ACS Photonics* **2015**, *2*, 921.

(36) Atre, A. C.; Brenny, B. J. M.; Coenen, T.; García-etxarri, A.; Polman, A.; Dionne, J. A. Nanoscale Optical Tomography with Cathodoluminescence Spectroscopy. *Nat. Nanotechnol.* **2015**, *10*, 429−436.

(37) Aigouy, L.; De Wilde, Y.; Mortier, M. Local Optical Imaging of Nanoholes Using a Single Fluorescent Rare-Earth-Doped Glass Particle as a Probe Local Optical Imaging of Nanoholes Using a Single Fluorescent Rare-Earth-Doped Glass Particle as a Probe. *Appl. Phys. Lett.* **2003**, *83*, 147.

(38) Krachmalnicoff, V.; Cao, D.; Caz, A.; Castani, E.; Pierrat, R.; Collin, S.; Carminati, R.; Wilde, Y. De. Towards a Full Character-

ization of a Plasmonic Nanostructure with a Fluorescent near-Field Probe. *Opt. Express* **2013**, *21*, 11536.

(39) Cang, H.; Labno, A.; Lu, C.; Yin, X.; Liu, M.; Gladden, C.; Liu, Y.; Zhang, X. Hotspot by Single Molecule Imaging. *Nature* **2011**, *469*, 385−388.

(40) Wertz, E.; Isaaco, B. P.; Flynn, J. D.; Biteen, J. S. Single-Molecule Super-Resolution Microscopy Reveals How Light Couples to a Plasmonic Nanoantenna on the Nanometer Scale. *Nano Lett.* **2015**, *15*, 2662.

(41) Guo, K.; Verschuuren, M.; Koenderink, F. Superresolution Imaging of the Local Density of States in Plasmon Lattices. *Optica* **2016**, *3*, 32−39.

(42) Huang, B.; Wang, W.; Bates, M.; Zhuang, X. Three-Dimensional Super-Resolution Imaging by Stochastic Optical Reconstruction Microscopy. *Science (Washington, DC, U. S.)* **2008**, *319*, 810.

(43) Frederiksen, R. S.; Alarcon-Llado, E.; Madsen, M.; Rostgaard, K.; Krogstrup, P.; Vosch, T.; Nygard, J.; Fontcuberta, I.; Morral, A.; Martinez, K. Modulation of Fluorescence Signals from Biomolecules along Nanowires due to Interaction of Light with Oriented Nanostructures. *Nano Lett.* **2015**, *15*, 176.

(44) Frederiksen, R. S.; Alarcon-llado, E.; Krogstrup, P.; Bojarskaite, L.; Buch-ma, N.; Bolinsson, J.; Nyga, J.; Fontcuberta, I.; Morral, A.; Martinez, K. L. Nanowire-Aperture Probe: Local Enhanced Fluorescence Detection for the Investigation of Live Cells at the Nanoscale. *ACS Photonics* **2016**, *3*, 1208.

(45) Nowzari, A.; Heurlin, M.; Jain, V.; Storm, K.; Hosseinnia, A.; Anttu, N. A Comparative Study of Absorption in Vertically and Laterally Oriented InP Core−Shell Nanowire Photovoltaic Devices. *Nano Lett.* **2015**, *15*, 180910.1021/nl504559g.

(46) Wang, B.; Leu, P. W. Tunable and Selective Resonant Absorption in Vertical Nanowires. *Opt. Lett.* **2012**, *37*, 3756−3758.

(47) Fountaine, K. T.; Whitney, W.; Atwater, H. a. Resonant Absorption in Semiconductor Nanowires and Nanowire Arrays: Relating Leaky Waveguide Modes to Bloch Photonic Crystal Modes. *J. Appl. Phys.* **2014**, *116*, 153106.

(48) Novotny, L.; Van Hulst, N. Antennas for Light. *Nat. Photonics* **2011**, *5*, 83.

(49) Johlin, E.; Solari, J.; Mann, S. A.; Wang, J.; Shimizu, T. S.; Garnett, E. C. Super-Resolution Imaging of Light-matter Interactions near Single Semiconductor Nanowires. *Nat. Commun.* **2016**, *7*, 1−6.

(50) Kandziolka, M.; Charlton, J. J.; Kravchenko, I. I.; Bradshaw, J. A.; Merkulov, I. A.; Sepaniak, M. J.; Lavrik, N. V. Silicon Nanopillars As a Platform for Enhanced Fluorescence Analysis. *Anal. Chem.* **2013**, *85*, 9031.

(51) Wells, S.; Merkulov, I.; Kravchenko, I.; Lavrik, N.; Sepaniak, M. J. Silicon Nanopillars for Field-Enhanced Surface Spectroscopy. *ACS Nano* **2012**, *6*, 2948−2959.